DATA-DRIVEN QUASI-LINEAR MODELLING OF COMPRESSIBLE TURBULENT CHANNEL FLOWS USING INCOMPRESSIBLE DATA

Zecheng Zou
Department of Aeronautics
Imperial College London
South Kensington, London SW7 2AZ, UK
zecheng.zou19@imperial.ac.uk

Alessandro Ceci
Mathematics
Gran Sasso Science Institute
Viale Francesco Crispi 7, 67100 L'Aquila, Italy
alessandro.ceci@gssi.it

Sergio Pirozzoli
Dipartimento di Ingegneria Meccanica e Aerospaziale
Sapienza Università di Roma
Via Eudossiana, Roma 00184, Italy
sergio.pirozzoli@uniroma1.it

Yongyun Hwang
Department of Aeronautics
Imperial College London
South Kensington, London SW7 2AZ, UK
y.hwang@imperial.ac.uk

ABSTRACT

This study extends the data-driven quasi-linear approximation (DQLA) (Holford, Lee & Hwang, *J. Fluid Mech.*, 2024, 980:A12) to compressible turbulent channel flow. The DQLA employs the eddy-viscosity-enhanced linearised compressible Navier–Stokes operator (Chen et al., *J. Fluid Mech.*, 2023, 962:A7), driven by stochastic forcing whose streamwise weights are determined through self-similarity assimilated from incompressible direct numerical simulation (DNS) database, and spanwise weights are obtained by minimizing discrepancies in the turbulent fluxes between the mean and the fluctuation equations. Without any compressible DNS input, the extended DQLA reproduces turbulence intensities and spectra in close quantitative agreement with DNS up to bulk Mach number $Ma_b = 1.5$, and exhibits a consistent collapse of turbulence statistics across Ma_b when expressed in semi-local units at the same centreline semi-local friction Reynolds number $Re^*_{\tau c}$, consistent with Morkovin's hypothesis. The results demonstrate the predictive capability of the extended DQLA up to moderate Mach numbers, and establish its potential as a physically interpretable and computationally efficient framework for exploring compressible wall-bounded turbulence at high Reynolds numbers.

INTRODUCTION

Compressible wall-bounded turbulent flows are central in advancing high-speed aerospace technologies. A foundational framework for compressible turbulent flows is Morkovin's hypothesis (Morkovin, 1962), which posits that at moderate Mach numbers the turbulence retains incompressible-like characteristics if the density fluctuations remain small relative to their mean values. This idea underpins successful mapping strategies, such as the Van Driest transformation (Van Driest, 1951) and its subsequent refinements (Trettel & Larsson, 2016; Modesti & Pirozzoli, 2016; Volpiani *et al.*, 2020), which collapse compressible mean velocity and Reynolds stress profiles onto incompressible counterparts. Another important implication is the approximate linear relationship between velocity and temperature fluctuations, formalised as the strong Reynolds analogy (SRA) (Morkovin, 1962; Huang *et al.*, 1995), which links velocity and temperature fluctuations and remains central in compressible turbulence modelling.

In recent decades, the linearised Navier–Stokes (LNS) equations have emerged as powerful tools for modelling and analysing turbulence (Hwang & Cossu, 2010; Alizard *et al.*, 2015; Ran *et al.*, 2021). Among these, the quasi-linear approximation (QLA) provides a framework to incorporate nonlinearity in a controlled manner by decomposing the flow into a mean state and fluctuation state, where self-interacting terms are modelled (Malkus, 1954; Farrell & Ioannou, 2003; Marston *et al.*, 2008; Thomas *et al.*, 2014). A notable development is the minimal quasi-linear approximation (MQLA) (Hwang & Eckhardt, 2020), which is designed on the attached eddy model and successfully predicts the turbulence intensity and spectra. More recently, this approach has been extended to provide a complete description of turbulence statistics and spectra by improving the form of stochastic forcing using DNS data (Holford *et al.*, 2024).

In this study, we exploit Morkovin's hypothesis and modified SRA to extend QL framework of Holford *et al.* (2024), informed by incompressible DNS data, to model turbulent fluctuations in compressible channel flow.

PROBLEM FORMULATION

Equation of Motion and Stress Modelling

We consider a pressure-driven compressible turbulent channel flow of a perfect gas between two isothermal, no-slip walls. The governing equations are decomposed into mean and fluctuating components using the Favre (density-weighted) averaging.

We adopt a common approximation in compressible turbulence studies (Huang *et al.*, 1995; Gatski & Bonnet, 2013), retaining the leading contributions of molecular viscosity and thermal conductivity in the mean equations. For statistically homogeneous channel flow, the mean equations of mass and streamwise momentum can be reduced to

$$\overline{\rho' v''} = 0, \tag{1}$$

$$\widetilde{u''v''} \approx \frac{1}{\bar{\rho}}\left(\frac{\tilde{\mu}}{Re_b}\frac{\partial \tilde{u}}{\partial y} - \tau_w(1-\frac{y}{h})\right). \quad (2)$$

Here, τ_w is the mean wall shear stress, and $\bar{()}$ and $\widetilde{(\cdot)}$ denote time and Favre average, respectively. For temperature closure, turbulent flux $\widetilde{v''T''}$ is modeled using modified SRA (Huang *et al.*, 1995) with turbulent Prandtl number $Pr_t = 1$ as

$$\widetilde{v''T''} = \frac{1}{\bar{\rho}}\left(\frac{\partial \tilde{T}}{\partial y}\bigg/\frac{\partial \tilde{U}}{\partial y}\right)\left(\frac{\tilde{\mu}}{Re_b}\frac{\partial \tilde{u}}{\partial y} - \tau_w(1-\frac{y}{h^d})\right). \quad (3)$$

Following Chen *et al.* (2023), in the fluctuation equations, the nonlinear terms associated with the fluctuations of Reynolds stress and turbulent heat flux are modelled using the linearised Boussinesq assumption and modified SRA. The remaining nonlinear terms directly involving density fluctuations are considered as secondary in importance, consistent with the spirit of Morkovin's hypothesis, and are absorbed into a stochastic forcing. The resulting fluctuation equations for the quasi-linear approximation are

$$\frac{\partial q''}{\partial t} = \mathscr{L}_{eLNS} q'' + f''_{eLNS}, \quad (4)$$

where $q = [\rho, u, v, w, T]^T$, $\mathscr{L}_{eLNS}$ is the linear operator containing all linear terms, and $f''_{eLNS} = [f''_\rho, f''_u, f''_v, f''_w, f''_T]^T$ denotes the stochastic forcing.

Turbulent Mean Flow

The mean profiles of velocity $\tilde{u}$ and temperature $\tilde{T}$ are obtained from the ODE-based model of Chen *et al.* (2023). This model solves a set of ordinary differential equations derived from commonly used relations in compressible mean-flow modelling to produce accurate profiles up to $Ma_b = 5$ and $Re_\tau = 10^5$ without relying on DNS data.

Forcing Construction and QL Approximations

The forcing in (4) is first assumed to be white in time and uncorrelated in the wall-normal direction, such that

$$\mathbb{E}_F[\hat{f}(t,y;k_x,k_z)\hat{f}^H(t',y';k_x,k_z)] = \mathbf{W}\delta(y-y')\delta(t-t'), \quad (5)$$

where $\mathbf{W} = \mathrm{diag}\{W_\rho, W_u, W_v, W_w, W_T\}$ denotes the undetermined weights of each forcing component. $\mathbb{E}_F[\cdot]$ represents the Favre ensemble average, and the Dirac delta functions represent decorrelation in both wall-normal direction and time.

With the stochastic forcing driven, the resulting power- and cross-spectral covariance of the fluctuation q'' can be obtained from

$$\phi_{qq}(y,y';k_x,k_z) = \mathbb{E}_F\left[\hat{q}(y,t;k_x,k_z)\hat{q}^H(y',t;k_x,k_z)\right]. \quad (6)$$

Given the linear relationship between forcing and response, the spectral covariance ϕ_{qq} can be decomposed into the contributions from each forcing component (Jovanović & Bamieh, 2005; Chen *et al.*, 2023; Holford *et al.*, 2024) as

$$\phi_{qq}(y,y';k_x,k_z) = \sum_{r=\rho,u,v,w,T} W_r(k_x,k_z)\phi_{qq,r}(y,y';k_x,k_z), \quad (7)$$

where $\phi_{qq,r}$ is the spectral covariance matrix of the response q'' associated with each component of the forcing with the unit amplitude.

Due to the statistically homogeneous nature in the streamwise and spanwise directions, and following Holford *et al.* (2024), the undertermined weight $W_r(k_x,k_z)$ is further decomposed as

$$W_r(k_x,k_z) = W_{l,k_z}(k_z)W_{r,k_x}(k_x/k_z), \quad (8)$$

where $W_{l,k_z}(k_z)$ with $l = \{\rho, m, T\}$ and $W_{r,k_x}(k_z/k_x)$ with $r = \{\rho, u, v, w, T\}$ are the spanwise and streamwise weights, respectively.

The streamwise weights for the velocity components u, v, w are determined from incompressible DNS data based on self-similarity in the logarithmic region (Holford *et al.*, 2024), consistent with the spirit of attached eddy hypothesis (Townsend, 1976). For temperature and density components, the modified SRA (Huang *et al.*, 1995) implies scaling with the streamwise velocity, thus their weights may be taken directly from that of the streamwise velocity, i.e.

$$W_{\rho,k_x}(k_x/k_z) = W_{T,k_x}(k_x/k_z) = W_{u,k_x}(k_x/k_z). \quad (9)$$

With these specifications, the final form of the response spectral covariance matrix is written as follows:

$$\phi_{qq}(y,y';k_x,k_z) = \sum_{n=\rho,T} W_{n,k_z}(k_z)\,W_{n,k_x}(k_x/k_z)\,\phi_{qq,n}^{N_{\mathrm{POD}}}(y,y';k_x,k_z) + W_{u,k_z}(k_z)\sum_{m=u,v,w} W_{m,k_x}(k_x/k_z)\,\phi_{qq,m}^{N_{\mathrm{POD}}}(y,y';k_x,k_z). \quad (10)$$

Finally, the spanwise weights $W_{l,k_z}(k_z)$ are determined by solving an optimisation problem which minimises the differences between the turbulent fluxes from (1), (2) and (3) and those computed from the fluctuation equations.

$$\min_{W_{l,k_z}} \sum_{l=\{\rho,u,T\}}\left[J_l^{0.5} + \gamma_l\left(\int_0^\infty\left(\frac{d^2W_{l,k_z}(k_z)}{d(\ln k_z)^2}\right)^2 dk_z\right)^{0.5}\right], \quad (11a)$$

where

$$J_\rho = \int_0^2\left(\mathbb{E}_F[\rho'v''](y)\right)^2 Q(y)\,dy, \quad (11b)$$

$$J_u = \frac{\int_0^2\left(\widetilde{u''v''}(y) - \mathbb{E}_F[u''v''](y)\right)^2 Q(y)\,dy}{\int_0^2\left(\widetilde{u''v''}(y)\right)^2 Q(y)\,dy}, \quad (11c)$$

$$J_T = \frac{\int_0^{2h}\left(\widetilde{v''T''}(y) - \mathbb{E}_F[v''T''](y)\right)^2 Q(y)dy}{\int_0^2\left(\widetilde{v''T''}(y)\right)^2 Q(y)\,dy}, \quad (11d)$$

subject to

$$W_{l,k_z}(k_z) \geq 0. \quad (11e)$$

Here, $Q(y) = (1-|\eta|)^{-1}$ with $\eta = y-1$ is the integration weight, and $\mathbb{E}_F[u''v''](y)$ is computed from

$$\mathbb{E}_F[u''v''](y) = \frac{1}{4\pi^2}\int_0^{2h}\int_0^\infty\int_0^\infty \phi_{uv}(y,y';k_x,k_z,)\delta(y'-y)\,dk_x\,dk_z\,dy'. \quad (12)$$

The resulting optimisation problem is formulated in the standard form of a second-order cone program and is solved to obtain the spanwise weights. Once the streamwise and spanwise weights are determined, the turbulence statistics of compressible channel flow can be reconstructed efficiently.

COMPARISON WITH DNS

We compare DNS and DQLA results at the same friction Reynolds number ($Re_\tau \approx 1000$) and the same semi-local friction Reynolds number ($Re^*_{\tau c} \approx 340$) for incompressible, $Ma_b = 0.8$ and 1.5 cases.

Figure 1 compares the turbulence intensities of streamwise velocity and Reynolds stress from DNS and DQLA at $Re_\tau \approx 1000$. Up to $Ma_b = 1.5$, DQLA reproduces turbulence statistics in close agreement with DNS. In figure 1(a,b), the Reynolds shear stress profiles peak at consistent wall-normal locations and achieve nearly identical magnitudes, indicating that DQLA accurately captures the mean momentum balance in (2) under moderate compressibility - this is expected, given the accuracy of the mean velocity profiles from the ODE-based model. In figure 1(c,d), the streamwise intensity u^*_{rms} increases with Ma_b and its peak also shifts progressively towards the channel centreline. Moreover, the amplitudes of the streamwise velocity fluctuation predicted by DQLA match the DNS results well, demonstrating its ability to capture the anisotropic distribution of turbulent kinetic energy effectively.

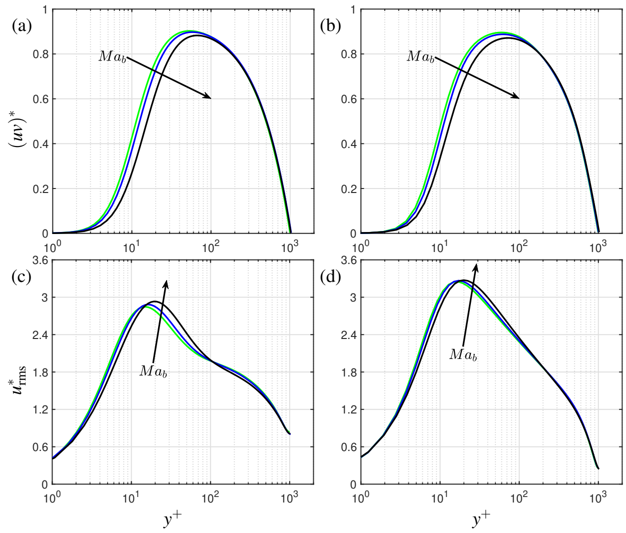

Figure 1: Comparison between (a,c) DNS and (b,d) DQLA at $Re_\tau \approx 1000$ for incompressible (green), $Ma_b = 0.8$ (blue), 1.5 (black). Here, (a,b) Reynolds shear stress; (c,d) streamwise rms velocity.

Figure 2 compares the premultiplied one-dimensional spanwise spectra of streamwise velocity and Reynolds stress from DNS and DQLA at $Re_\tau \approx 1000$. Overall, DQLA successfully reproduces the qualitative shape and orientation of the energetic ridges observed in the DNS results. In both components, the energy is primarily concentrated along an approximately linear ridge for both DNS and DQLA. In particular, the energy ridges approximately follow a linear scaling relationship between the wall-normal distance and the spanwise wavelength, the typical characteristics associated with the presence of self-similar wall-attached eddy structures (Hwang, 2015). This finding supports the physical relevance of adopting self-similar streamwise weights in modelling compressible channel turbulence.

Figure 3 shows the turbulence intensities of streamwise velocity and Reynolds stress from DNS and DQLA at $Re^*_{\tau c} \approx 340$. The Reynolds shear stress profiles of both DNS and DQLA collapse effectively in semi-local units. The streamwise turbulence intensity in compressible cases consistently exceeds that of incompressible flow, especially near the peak location at $y^* \approx 15$, where the peak intensity slowly increases with Ma_b (figure 3(c,d)). These variations are manifestations of intrinsic compressibility effects, which have been analysed

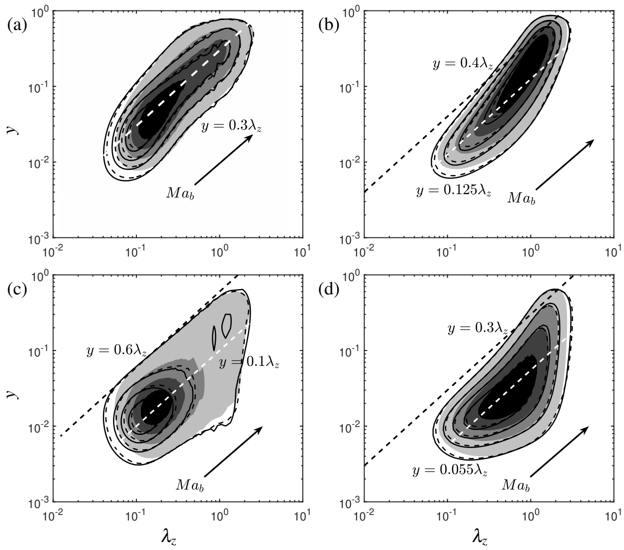

Figure 2: Premultiplied spanwise-wavenumber spectra from (a,c) DNS and (b,d) DQLA at $Re_\tau = 1000$: (a,b) streamwise velocity; (c,d) Reynolds shear stress. Incompressible and $Ma_b = 0.8, 1.5$ correspond to the solid, dashed and shaded line contours, respectively. Contours at 0.2, 0.4, 0.6 and 0.8 of the maximum.

in detail based on DNS by Hasan *et al.* (2025).

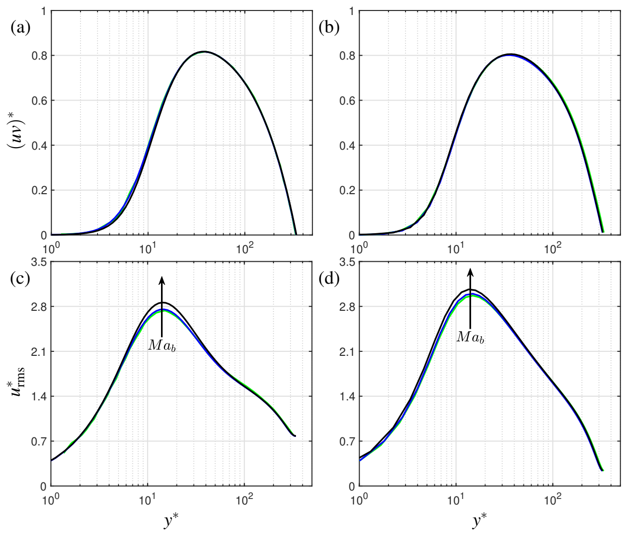

Figure 3: Comparison between (a,c) DNS and (b,d) DQLA at $Re^*_{\tau c} \approx 340$ for incompressible (green), $Ma_b = 0.8$ (blue), 1.5 (black). Here, (a,b) Reynolds shear stress; (c,d) streamwise rms velocity.

Figure 4 compares the premultiplied one-dimensional streamwise spectra of DQLA at $Ma_b = 0.8$ and 1.5 with the reference incompressible DQLA (Holford *et al.*, 2024) at $Re^*_{\tau c} \approx 340$, expressed in the semi-local unit: i.e. the wavelengths are scaled as $\lambda^*_x = 2\pi/k^*_x$ and $\lambda^*_z = 2\pi/k^*_z$. In figure 4(a,b), the DQLA spectra at both Mach numbers exhibit excellent collapse with the reference incompressible case. These observations are consistent with the recent DNS findings reported by Yao & Hussain (2020), who demonstrated that premultiplied streamwise and spanwise spectra at $Ma_b = 1.5$ collapse well with incompressible cases in the semi-local units when the same $Re^*_{\tau c}$ is considered. The consistent behaviour of DNS results indicates that the self-similarity, originally retrieved from incompressible flow, is still valid in semi-local units at moderate Mach number. Therefore, the factorised weight decomposition adopted here and the streamwise weights inherited from incompressible self-similarity remain reasonable assumptions at moderate Mach number. The observed collapse of the DQLA spectra further indicates that the linearised operator used for turbulent fluctuations in the present study captures the important compressibility effects, supporting Morkovin's hypothesis in wall-bounded flows.

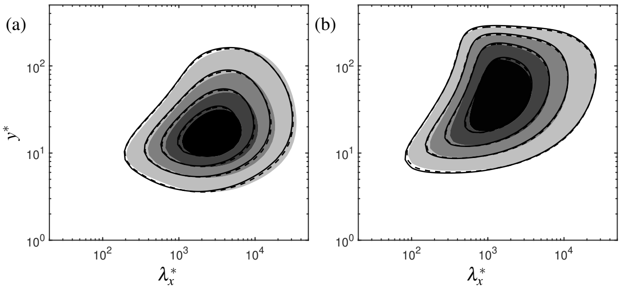

Figure 4: Premultiplied streamwise-wavenumber spectra from DQLA in semi-local units at $Re^*_{\tau c} \approx 340$: (a) streamwise velocity and (b) Reynolds shear stress. Incompressible and $Ma_b = 0.8, 1.5$ correspond to the solid, dashed and shaded line contours, respectively. Contours at 0.2, 0.4, 0.6 and 0.8 of the maximum.

ANALYSIS OF SEMI-LOCAL COLLAPSE

As shown in figures 3 and 4, when scaled in semi-local units, the turbulence fluctuations and spectra from DQLA remain invariant with changes in Ma_b at the same semi-local friction Reynolds number $Re^*_{\tau c}$. These behaviours are consistent with Morkovin's hypothesis and observations from DNS. In the following, we discuss how this semi-local collapse is incorporated into DQLA.

First, it is well established that the mean flow profiles of turbulent channel flow, at moderate and even high Mach numbers, collapse onto the reference incompressible case in semi-local units, when using appropriate compressibility transformations (Zhang *et al.*, 2014; Trettel & Larsson, 2016; Volpiani *et al.*, 2020; Griffin *et al.*, 2021). This property is also a cornerstone supporting Morkovin's hypothesis. The ODE-based model employed in the present study (Chen *et al.*, 2023) uses the compressibility transformation developed by Trettel & Larsson (2016). The resulting mean flow profiles also achieve collapse when expressed in semi-local units. This inherent characteristic of the mean profiles, although not directly involving the quasi-linear dynamics, forms the foundation for the collapse of turbulence statistics in DQLA.

With these ODE-based mean flow profiles as input, the shape functions of the response POD modes from eLNS operator at $k_x = 0$ for different Mach numbers are compared in figure 5. Under white-in-time forcing uncorrelated in the wall-normal direction, the response mode shapes show the intrinsic collapse when scaled in semi-local units. Both the inner-peak mode at $\lambda^*_{z,c} = 100$ and the outer-peak mode at $\lambda_z = 3.7h$ exhibit good collapse. This similarity indicates that the eLNS operator respects the semi-local scaling embedded in the mean flow at the moderate Mach number.

In DQLA, the streamwise and spanwise weights for the forcing, $W_{r,k_x}(k_z/k_x)$ and $W_{l,k_z}(k_z)$, directly determine the amplitudes of two-dimensional spectra. First, the streamwise weight $W_{r,k_x}(k_z/k_x)$ is assimilated from incompressible DNS data, and its parameter k_x/k_z represents the self-similarity in the wavenumber space. We note that this parameter is dimensionless and depends on whether the relationship between wavenumber pairs observed in incompressible flows remains valid at moderate Mach number, which is consistent with the spirit of Morkovin's hypothesis. Second, the spanwise weights $W_{l,k_z}(k_z)$ are determined by fitting the turbulent fluxes derived from the mean profiles within an active spanwise wavenumber range. This fitting procedure ensures that the total turbulent flux response is consistent with the corresponding fluxes $\widetilde{u''v''}$ and $\widetilde{v''T''}$ derived from the mean profiles, which are known to collapse in the semi-local unit in the wall-normal direction.

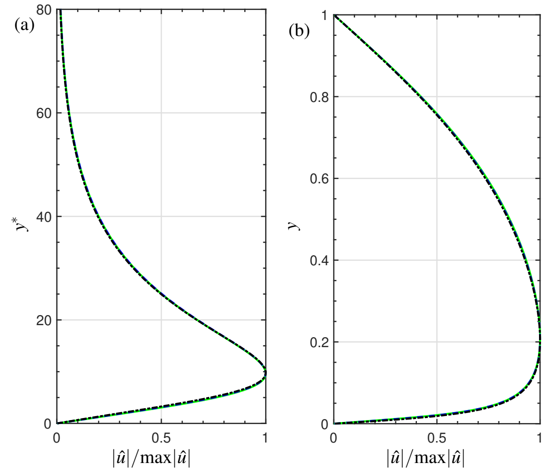

Figure 5: Comparison of shape function of streamwise response at $k_x = 0$ for the mode at the (a) inner peak ($\lambda^*_{z,c} = 100$) and (b) outer peak ($\lambda_z = 3.7h$). Here, these cases are at $Re^*_{\tau c} \approx 340$ for incompressible case (green solid), $Ma_b = 0.8$ (blue dashed), and 1.5 (black dash-dotted).

The discussion above suggests that all these modelling elements originate from the mean flow profiles, which are approximately invariant under the compressibility transformation, except for the dimensionless streamwise weight $W_{r,k_x}(k_x/k_z)$. This weight may be viewed as a direct input to the fluctuation model governing the quasi-linear dynamics. Therefore, when the Mach number is moderate, such that coupling between the velocity and temperature fields is weak, it is reasonable to presume that the linear fluctuation model in DQLA is largely slaved to the scaling properties of the mean flow.

HIGH-REYNOLDS-NUMBER EFFECT PREDICTIONS AT MACH 1.5

Using its predictive capability across all Reynolds numbers, DQLA is extended for Re_τ ranging from 5×10^2 to 5×10^3 (i.e. $Re^*_{\tau c} \approx 340 \sim 3400$) at $Ma_b = 1.5$.

Figure 6 shows the streamwise premultiplied one-dimensional spectra from DQLA at $Re^*_{\tau c} \approx 340, 680$, and 1340, scaled with the inner (λ^*, y^*) and outer (λ/h, y/h) units. Despite minor quantitative discrepancies at individual Reynolds numbers, the overall scaling behaviours are in good agreement with DNS. The spectra are energetic over the scales from $\lambda^*_x = \mathscr{O}(10^2)$ to $\lambda_x/h = \mathscr{O}(10)$. When scaled in inner units, both the streamwise velocity and Reynolds shear stress spectra exhibit a clear collapse over a wide range of λ^*_x and y^*, consistent with the incompressible case reported by Holford *et al.* (2024), and thereby supporting the semi-local rescaling. It is worth noting that the streamwise velocity spectra at different Reynolds numbers exhibit an inner peak at $y^* \approx 15$ and $\lambda^* \sim O(1000)$, which corresponds to the characteristic scale of near-wall streaks (Hwang, 2015). When scaled in outer units, the outer part of the spectra also collapses well, indicating that the outer-layer structures follow a consistent outer-layer scaling. The Reynolds-number scaling captured by DQLA agrees well with that found in the DNS study of Yao & Hussain (2020).

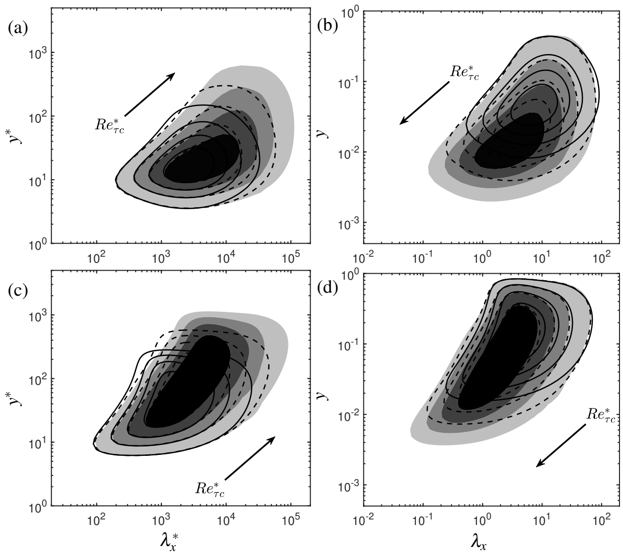

Figure 6: (a,c) Inner- and (b,d) outer-scaled premultiplied streamwise wavenumber spectra from DQLA at $Ma_b = 1.5$: (a,b) streamwise velocity and (c,d) Reynolds shear stress. Here, the $Re^*_{\tau c} = 337, 684, 1343$ cases correspond to the solid, dashed, and shaded line contours, respectively. The contour levels are chosen as 0.2, 0.4, 0.6 and 0.8 times the maximum value.

Figure 7 compares the scaling behaviour of the streamwise turbulence intensity from DNS (Yao & Hussain, 2020) and DQLA at fixed $Ma_b = 1.5$, in outer- and inner-scaled coordinates. DQLA quantitatively captures the Reynolds-number scaling trends observed in DNS. In the outer units (figure 7(a,b)), the streamwise turbulence intensity exhibits an approximate logarithmic decay, which is consistent with DNS. This logarithmic wall-normal dependence becomes more pronounced as the Reynolds number increases to higher $Re^*_{\tau c} \approx 3400$. With the theoretical prediction of Townsend (1976) and Perry & Chong (1982), the streamwise turbulence intensity profiles of DQLA can be approximately represented as,

$$(uu)^* = A\ln(y) + B, \tag{13}$$

where A and B are constants (see the black dashed line in figure 7(b)). It is worth noting that the Reynolds number has recently been shown to slowly affect A and B due to the small viscous effect (Hwang *et al.*, 2022). However, this issue is not pursued further given the narrow range considered here. In the inner units (figure 7(c,d)), both DNS and DQLA exhibit a near-wall peak in the streamwise turbulence intensity at $y^* \approx 15$, which remains approximately independent of the Reynolds number within the range of the Reynolds number considered. This behaviour is consistent with previous incompressible DNS and DQLA results, where the peak also occurs

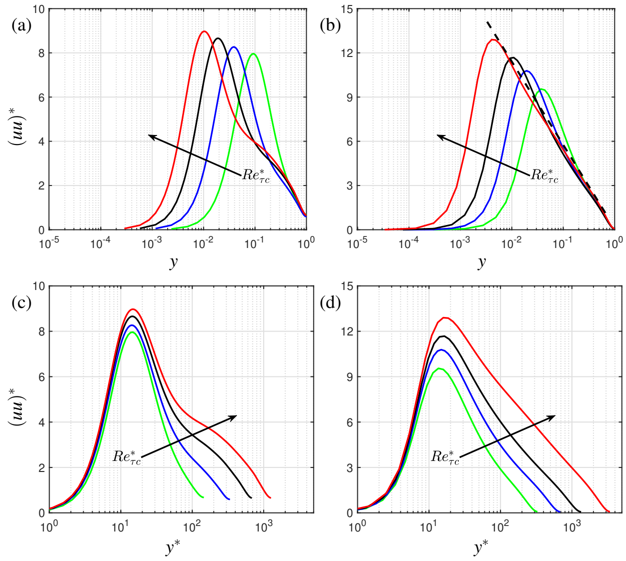

Figure 7: Streamwise turbulence intensity profiles from (a,c) DNS (Yao & Hussain, 2020) and (b,d) the DQLA in (a,b) outer-scaled units and (c,d) inner-scaled units. Here, $Re^*_{\tau c} = 145, 337, 683, 1266$ for DNS and $Re^*_{\tau c} = 337, 684, 1343, 3404$ for the DQLA. Here, the dashed line in (b) denotes scaling of $A\ln(y) + B$, with $A = -2.45$ and $B = 0.12$.

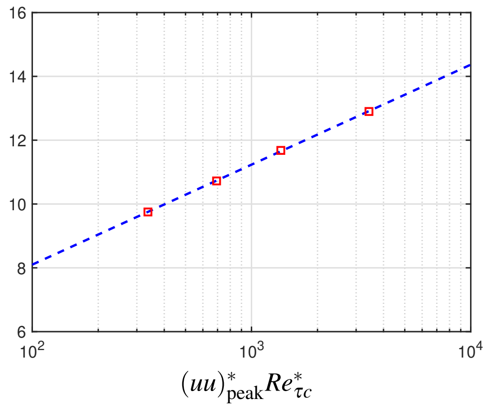

Figure 8: Peak values of streamwise turbulence intensity as a function of $Re^*_{\tau c}$ from the DQLA. Here, the blue dashed lines denotes scaling of $C\log(Re^*_{\tau c}) + D$, with $C = 1.36$ and $D = 1.83$.

at $y^+ \approx 15$ at relatively low Reynolds numbers ($Re_\tau \lesssim 5000$) (Lee & Moser, 2015; Holford *et al.*, 2024).

Finally, figure 8 examines the scaling of the near-wall peak streamwise turbulence intensity $(uu)^*_{\text{peak}}$ at $Ma_b = 1.5$. The present DQLA results are found to follow the approximate logarithmic relation $(uu)^*_{\text{peak}} = C\log(Re^*_{\tau c}) + D$ (C and D are constants), which is reported by Yao & Hussain (2020) from DNS for $Re^*_{\tau c} \lesssim 1300$, and this scaling appears to remain vaild for $Re^*_{\tau c} \lesssim 3400$.

CONCLUSIONS AND FUTURE WORK

The present study extends the data-driven quasi-linear approximation, originally developed for incompressible turbulent channel flows (Hwang & Eckhardt, 2020; Holford *et al.*, 2024), to compressible channel flows at moderate Mach numbers. The extension builds on streamwise weights assimilated from incompressible DNS data at $Re_\tau \approx 5200$ (Holford *et al.*, 2024), exploiting the self-similarity of the velocity spectra and employing the strong Reynolds analogy proposed by Huang *et al.* (1995). The spanwise weights are determined by matching the target turbulent fluxes from the linearised fluctuation model to those obtained from the mean equations. This approach enables DQLA predictions for $Ma_b \leq 1.5$ over a wide range of Reynolds numbers.

Comparisons with DNS demonstrate that DQLA reproduces key turbulence statistics and spectral characteristics with reasonable accuracy, confirming the validity of Morkovin's hypothesis at moderate Mach number. At fixed Re_τ, DQLA also captures the Mach-number trends observed in DNS. At the matched $Re^*_{\tau c}$, both turbulence intensities and energy spectra show excellent collapse across different Mach numbers, when scaled using semi-local units. Essential spectral features, such as the attached-eddy footprints, and the characteristic near-wall peak at $y^* \approx 15$ are also captured well.

The extended compressible DQLA, with strong predictive capabilities across different Reynolds numbers, provides an efficient and physically consistent approach for modelling turbulence fluctuation statistics and energy spectra at moderate Mach number. While DNS typically requires several days of computation on the $\mathscr{O}(10^3)$ CPUs, DQLA is able to reconstruct these turbulence statistics within minutes using a single CPU. Future work will aim to extend the DQLA framework to higher Mach numbers and to non-isothermal wall conditions.

REFERENCES

Alizard, F., Pirozzoli, S., Bernardini, M. & Grasso, F. 2015 Optimal transient growth in compressible turbulent boundary layers. *J. Fluid Mech.* **770**, 124–155.

Chen, X., Cheng, C., Fu, L. & Gan, J. 2023 Linear response analysis of supersonic turbulent channel flows with a large parameter space. *J. Fluid Mech.* **962**, A7.

Farrell, B.F. & Ioannou, P.J. 2003 Structural stability of turbulent jets. *J. Atmos. Sci.* **60**, 2101–2118.

Gatski, T. B. & Bonnet, J.-P. 2013 *Compressibility, Turbulence and High Speed Flow*. Amsterdam,Netherlands: Academic Press.

Griffin, K.P., Fu, L. & Moin, P. 2021 Velocity transformation for compressible wall-bounded turbulent flows with and without heat transfer. *Proc. Natl Acad. Sci. USA* **118** (34), e2111144118.

Hasan, A.M., Costa, P., Larsson, J., Pirozzoli, S. & Pecnik, R. 2025 Intrinsic compressibility effects in near-wall turbulence. *J. Fluid Mech.* **1006**, A14.

Holford, J.J., Lee, M. & Hwang, Y. 2024 A data-driven quasi-linear approximation for turbulent channel flow. *J. Fluid Mech.* **980**, A12.

Huang, P.G., Coleman, G.N. & Bradshaw, P. 1995 Compressible turbulent channel flows: Dns results and modelling. *J. Fluid Mech.* **305**, 185–218.

Hwang, Y. 2015 Statistical structure of self-sustaining attached eddies in turbulent channel flow. *J. Fluid Mech.* **767**, 254–289.

Hwang, Y. & Cossu, C. 2010 Linear non-normal energy amplification of harmonic and stochastic forcing in the turbulent channel flow. *J. Fluid Mech.* **664**, 51–73.

Hwang, Y. & Eckhardt, B. 2020 Attached eddy model revisited using a minimal quasi-linear approximation. *J. Fluid Mech.* **894**, A23.

Hwang, Y., Hutchins, N. & Marusic, I. 2022 The logarithmic variance of streamwise velocity and k^{-1} conundrum in wall turbulence. *J. Fluid Mech.* **933**, A8.

Jovanović, M.R. & Bamieh, B. 2005 Componentwise energy amplification in channel flows. *J. Fluid Mech.* **534**, 145–183.

Lee, M. & Moser, R.D. 2015 Direct numerical simulation of turbulent channel flow up to $Re_\tau \approx 5200$. *J. Fluid Mech.* **774**, 395–415.

Malkus, W.V.R. 1954 The heat transport and spectrum of thermal turbulence. *Proc. R. Soc. Lond. A* **225** (1161), 196–212.

Marston, J.B., Conover, E. & Schneider, T. 2008 Statistics of an unstable barotropic jet from a cumulant expansion. *J. Atmos. Sci.* **65**, 1955–1966.

Modesti, D. & Pirozzoli, S. 2016 Reynolds and mach number effects in compressible turbulent channel flow. *Intl J. Heat Fluid Flow* **59**, 33–49.

Morkovin, M.V. 1962 Effects of compressibility on turbulent flows. *In Mécanique de la Turbulence (ed. A. Favre)* **26**, 367–380.

Perry, A. E. & Chong, M. S. 1982 On the mechanism of wall turbulence. *J. Fluid Mech.* **119**, 173–217.

Ran, W., Zare, A. & Jovanović, M.R. 2021 Model-based design of riblets for turbulent drag reduction. *J. Fluid Mech.* **906**, A7.

Thomas, V. L., Lieu, B. K., Jovanović, M. R., Farrell, B. F., Ioannou, P. J. & Gayme, D. F. 2014 Self-sustaining turbulence in a restricted nonlinear model of plane Couette flow. *Physics of Fluids* **26** (10).

Townsend, A. A.R. 1976 *The Structure of Turbulent Shear Flow*. Cambridge University Press.

Trettel, A. & Larsson, J. 2016 Mean velocity scaling for compressible wall turbulence with heat transfer. *Phys. Fluids* **28** (2), 026102.

Van Driest, E.R. 1951 Turbulent boundary layer in compressible fluids. *J. Aeronaut. Sci.* **18** (3), 145–160.

Volpiani, P.S., Iyer, P.S., Pirozzoli, S. & Larsson, J. 2020 Data-driven compressibility transformation for turbulent wall layers. *Phys. Rev. Fluids* **5** (5), 052602.

Yao, J. & Hussain, F. 2020 Turbulence statistics and coherent structures in compressible channel flow. *Phys. Rev. Fluids* **5**, 084603.

Zhang, Y., Bi, W., Hussain, F. & She, Z. 2014 A generalized reynolds analogy for compressible wall-bounded turbulent flows. *J. Fluid Mech.* **739**, 392–420.